



Article

Enhanced MPPT-Based Fractional-Order PID for PV Systems Using Aquila Optimizer

Mohammed Tadj ¹, Lakhdar Chaib ¹, Abdelghani Choucha ¹, Al-Motasem Aldaoudeyeh ², Ahmed Fathy ^{3,4} , Hegazy Rezk ⁵ , Mohamed Louazni ^{6,*} and Attia El-Fergany ^{4,*}

- ¹ Energy and Materials Laboratory, University of Tamanghasset, Tamanghasset 11001, Algeria; m.tadj@mail.lagh-univ.dz (M.T.)
² Department of Electrical Power & Mechatronics Engineering, Tafilah Technical University, Tafilah 66110, Jordan; al-motasem@ttu.edu.jo
³ Department of Electrical Engineering, Jouf University, Sakaka 72388, Saudi Arabia; afali@ju.edu.sa
⁴ Electrical Power and Machines Engineering Department, Zagazig University, Zagazig 44519, Egypt
⁵ Department of Electrical Engineering, College of Engineering in Wadi Al-dawasir, Prince Sattam bin Abdulaziz University, Al-Kharj 11942, Saudi Arabia; hr.hussien@psau.edu.sa
⁶ Science Engineer Laboratory for Energy, National School of Applied Sciences, Chouaib Doukkali University of El Jadida, El Jadida P.O. Box 20, Morocco
* Correspondence: louazni.m@ucd.ac.ma (M.L.); el_fergany@zu.edu.eg (A.E.-F.)

Abstract: This paper proposes a controller to track the maximum power point (MPP) of a photovoltaic (PV) system using a fractional-order proportional integral derivative (FOPID) controller. The employed MPPT is operated based on a dP/dV feedback approach. The designed FOPIID-MPPT method includes a differentiator of order (μ) and integrator of order (λ), meaning it is an extension of the conventional PID controller. FOPIID has more flexibility and achieves dynamical tuning, which leads to an efficient control system. The contribution of our paper lies in optimizing FOPIID-MPPT parameters using Aquila optimizer (AO). The obtained results with the proposed AO-based FOPIID-MPPT are contrasted with those acquired with moth flame optimizer (MFO). The performance of our FOPIID-MPPT controller with the conventional technique perturb and observe (P&O) and the classical PID controller is analyzed. In addition, a robustness test is used to assess the performance of the FOPIID-MPPT controller under load variations, providing valuable insights into its practical applicability and robustness. The simulation results clearly prove the superiority and high performance of the proposed control system to track the MPP of PV systems.

Keywords: PV system; MPPT techniques; FOPIID; PID; Aquila optimizer; moth flame optimizer



Citation: Tadj, M.; Chaib, L.; Choucha, A.; Aldaoudeyeh, A.-M.; Fathy, A.; Rezk, H.; Louazni, M.; El-Fergany, A. Enhanced MPPT-Based Fractional-Order PID for PV Systems Using Aquila Optimizer. *Math. Comput. Appl.* **2023**, *28*, 99. <https://doi.org/10.3390/mca28050099>

Academic Editor: Guillermo Valencia-Palomo

Received: 9 August 2023

Revised: 27 September 2023

Accepted: 28 September 2023

Published: 3 October 2023



Copyright: © 2023 by the authors. Licensee MDPI, Basel, Switzerland. This article is an open access article distributed under the terms and conditions of the Creative Commons Attribution (CC BY) license (<https://creativecommons.org/licenses/by/4.0/>).

1. Introduction

Solar electricity production is one of the renewable energies used as a suitable solution due to growing energy demands. It is a clean, eco-friendly, and noiseless form of energy with an abundant fuel source. PV energy has become popular in energy generation due to its renewability, sustainability, affordability, and low maintenance [1].

A PV system comprises solar modules, a DC–DC converter, and load/battery/grid interconnections. PV system devices should be employed in a cooperative operation system to enhance the system's efficiency. A control scheme is used to keep the PV module operating at the maximum power point (MPP). This process of MPP operation is called maximum power point tracking (MPPT) [2,3].

The power–voltage (P–V) and current–voltage (I–V) curves of a solar cell are nonlinear. Indeed, the irradiance level variations influence the output voltage values, while the temperature changes influence the output current values [4]. In the P–V curve, there is one operating point represented as the MPP. The employment of a PV system with an MPP can attain the maximum energy production. This operating point on the P–V curve is unknown. Thus, an appropriate MPPT is required to reach this MPP [5,6].

Because of the changes in the switching frequency, the duty cycle parameter of the DC–DC converter varies, which leads to the PV module employment being near or at the MPP. Hence, control of the DC–DC converter switch may be achieved with conventional MPPT algorithms (i.e., perturb and observe (P&O) [7] and incremental conductance (IC) [8]) and soft computing MPPT algorithms based on artificial intelligence [9–11].

Over the recent years, the P&O algorithm has been widely used to track the MPP because of its simplicity and minimal computation parameters. The P&O technique compares two measured points to determine the perturbation orientation [12]. Numerous studies in the literature have been applied to enhance the P&O algorithm. A flower pollination algorithm (FPA) fortified with P&O is demonstrated in [13] and is based on a precise mathematical methodology. The scheme strategy was developed for maintaining the duty cycle to ensure the MPP. MPPT applying P&O in association with a fuzzy logic regulator used to regulate a boost converter is performed in [14] with the defined objective of comparing the output performance of a PV system. Mathi et al. exercised in [15] a combined global MPPT technique for obtaining a rapid and precise global MPP. This combination is an integration of the adjusted particle swarm optimizer (PSO) and P&O techniques. In [16], implementing a P&O MPPT-based method to control a buck-boost converter is applied. This converter assists in the switching of the PV voltage scale to perform the system's PV qualification within the supervision of a P&O approach. The proposed work in [17] achieves the maximum power point through secure independent PV modules and a battery system in order to provide an LED charge based on the MPPT approach using an improved variable step size P&O method. An enhanced control system is implemented in [18] to boost a PV converter using the MPPT sliding-mode technique in association with an inconstant-step-size P&O algorithm in the presence of partial shading states. Optimization techniques called cuckoo search and genetic algorithm are suggested in [19] in order to provide suitable controller gains for an MPPT-based P&O. In [20], a combination of two optimization techniques called shuffled frog leaping and pattern search is applied to tune an ANN to suit the MPP in a PV system. The P&O method is integrated to track an accurate MPP position after the optimization process of the ANN. In [21], an enhanced P&O algorithm is adopted under STC to reach the MPP with the best tracking, contrary to the traditional P&O technique. Kumar et al., in [7], employ an MPPT-based P&O technique to augment the effectiveness of a PV system with a buck-boost converter based on the nonlinear characteristic of current–voltage. In [22], a new P&O MPPT-based algorithm uses a reference PV cell attached at the top of a PV module to acquire data on the variation in current under variable climate conditions. In the case of attaining the MPP, the tracking and monitoring of the current variation in the reference PV cell is stopped. A combined boost converter is involved in [23] for achieving high system parameter efficiency. Moreover, a P&O-based MPPT method is used to control the converter by offering the maximum power. In [24], the effectiveness of the conventional P&O technique under fast variation in solar radiation with small and sizeable steps is studied. The MPPT technique based on an SMC is investigated in [25] for a PV system. An optimization algorithm named the krill herd algorithm has been suggested to adjust the SMC parameters to quickly track the MPP. In [26], Ali et al. proposed a modified P&O algorithm that divides the P–V allure into four zones according to the open-circuit voltage to rapidly track the MPP.

In terms of the IC algorithm, it proceeds better than the P&O method under non-uniform solar irradiation [27]. Practically, the IC algorithm can efficiently track the MPP better than the P&O algorithm. The IC algorithm can achieve the MPP, and the process achieves a steady-state phase and continues even with changes in the atmospheric conditions [12]. An MPPT-based IC approach was proposed in [28] to improve the effectiveness and profitability of PV system management. This approach is easy to implement and can segregate the immediate changes in voltage, current, and power during changes in the environmental conditions. Li et al. [29] implement a novel IC method to reach the MPP based on the power–voltage curve that is split into three regions: a region without an MPP, an MPP-comparable region, and an MPP region. To solve the MPPT tracking problem, the

work in [30] exercises an enhanced IC algorithm in coordination with a combined pattern search and crow search algorithm to tune neuro-fuzzy controller gains. Another study in [31] suggests a fast-tuning IC-MPPT for a PV system. The MPPT approach behavior is a combination of the effect of both the MPPT frequency interference and the step size caused by variation in the PV voltage. An MPPT algorithm is exposed in [32] based on a variable-step-size MPPT-IC algorithm, which instantaneously suits the following step size to boost the PV system's power. The study in [33] proposes a combination of the IC algorithm and PSO algorithm that keeps a large convergence scale in order to search for the maximum power point.

The researchers in [34] employ a thinned-out monitored MPPT based on IC to quickly follow the MPP in a PV module. A combined modeling predictive supervising scheme with an IC algorithm is involved to exploit the PV module at the MPP with autonomous PV system parameters [35]. An MPPT-based IC technique for controlling the reference output voltage and an adaptive reference regulator for monitoring the duty cycle interrupter of a DC–DC controller is proposed in [36]. In [37], a qualified MPPT algorithm is implemented using a fuzzy logic scheme, and a conventional IC technique for PV systems is presented. The proposed controller demonstrates efficient performance by employing tuned fuzzy logic gains to track the MPP. Another recent research work, described in [38], introduces an IC MPPT algorithm with two control levels. The first level sets the PV array's reference output voltage. The second monitoring loop uses an integral controller with a transfer function. Soft computing methods are an intriguing research area that involve creating intelligent computational systems exhibiting human-like characteristics such as learning, reasoning, and information processing. One such method is the artificial neural network (ANN), which is a computational learning technique inspired by the structure and functioning of the human neural network. In [39], Hiyama et al. propose an implementation of an ANN to estimate the MPP of a PV panel. Another study, described in [40], focuses on the development and application of a PC-based MPPT system for PV systems utilizing an ANN. In [41], a novel algorithm based on a backpropagation ANN is presented for effectively tracking the MPP. They show that ANNs surpass conventional MPPT techniques under varying solar radiance and temperature conditions. The proposed MPPT technique in [42] combines the use of an ANN to predict the general location of the global maximum power point and the conventional P&O technique for precise global maximum power point tracking. In [43], Ibelouad et al. introduce an algorithm that utilizes an ANN-based PSO technique. The ANN forecasts the solar irradiation and PV cell temperature, while the optimizer technique maximizes the power production and tracks the MPP. In [44], an intelligent MPPT algorithm is proposed, utilizing an ANN that is fine-tuned by three optimization algorithms to effectively track the MPP of a PV system. A comparison and analysis of MPPT approaches, including an ANN, fuzzy logic (FL), and P&O, are presented in [45] for MPP tracking. In order to accommodate the global MPP among multiple peaks, a novel ANN technique incorporating a radial basis function is suggested in [46] to predict the optimal global MPP. Haq et al., in [47], offer a controller based on a nonlinear global sliding mode to attain the maximum output power supplied by a PV module connected with a DC/DC converter. A feed-forward neural network is implemented to deliver a guide voltage and is developed to follow the ANN in order to produce a reference output under changing weather situations.

Fuzzy logic (FL) is an intelligent technique that utilizes membership degrees to determine the belongingness of an element to a particular set. It can be seen as an extension of crisp set theory. In [10], a research study proposes a control approach based on FL calculations for regulating the output of a PV converter. The objective is to extract the MPP under varying solar radiation conditions. In [48], an FL-based control strategy for MPPT is implemented to regulate a DC/DC converter and track the MPP of a PV system. The design and evaluation of a stand-alone PV system incorporating an FL-based MPPT-controlled DC–DC converter is presented [49]. Veeramanikandan et al. [50] demonstrate the performance of an MPPT algorithm based on the FL technique for monitoring a multi-

level inverter. This algorithm is applied to a PV inverter with segregated MPPT methods, especially in partial shading scenarios. Doubabi et al. [10] introduce a Takagi–Sugeno fuzzy logic system combined with multiple MPPT methods, offering fast, precise, and decisive MPPT tracking. In [51], the study presents an Internet-of-Things-based FL regulator for MPPT operation. Hai et al. [52] propose a combined MPPT technique utilizing FLC and an enhanced farmland fertility optimization technique to optimize the regulator gains in a PV system.

On the other hand, the optimization phase is a recently developed operation to maximize or minimize an objective function in a specific field by selecting the input parameters via a pre-defined situation. These optimizer techniques are fundamentally classified into biology-based, physics-based, and geography-based methods. Biology-based methods are mostly inspired from natural behaviors. They are also categorized into two groups, which are evolution-based methods and swarm-based methods. Examples of evolution-based methods are: genetic algorithms [53], evolutionary programming [54], and differential evolution [55]. Examples of swarm-based methods are: the particle swarm optimizer [56], bacteria foraging approach [57], artificial bee colony approach [58], cuckoo search approach [59], firefly algorithm [60], ant colony optimizer algorithm [61], and bird mating method [62]. Heuristics methods represent physics-based methods that mobilize imitations of the physical behavior of an issue. This group contains several techniques such as: the chaotic optimizer approach [63], simulated annealing technique [62], and immune system method [64]. Finally, geography-based methods are meta-heuristic methods that produce a random location inside the search space. An example of a geography-based method is the Tabu search algorithm [65].

The enhancement of a FOPID controller's degrees of freedom in the control law is directly related to the added fractional orders, i.e., the μ and λ parameters, which thus allows it to deal well with uncertainties in a PV system's parameters. The self-adjusting behavior of FOPID control gives it extra performance in order to improve the perturbation rejection aptitude of a PV system in contradiction to uncertain parameters and inputs [66]. Youcef et al. [67] suggest a stand-alone PV system operated with a new adaptive (A-FOPID) controller based on the self-adjusting of its parameters to gain the maximum power under changes in the ambient climate. A feed-forward neural network is applied to generate the appropriate voltage signal. Chen et al. [68] apply fractional calculus to a PV system to design a robust control concept. A DC/DC boost converter based on fractional order is established to augment the yield of the MPPT technique. An ANN is employed to constantly produce an efficient voltage signal.

In recent years, the MPPT-based dp/dv feedback approach has received a lot of consideration because it is relatively simple to implement and does not depend on the PV module's parameters [69]. Park et al. [70] present a practical application of the dp/dv technique to validate the effectiveness of an adjusted specified converter, which is further used with a microcontroller. The MPPT-based dp/dv feedback approach has additionally been implemented by varying the parameters of a PID regulator utilizing a fuzzy gain classifying method [71]. In [72], the effectiveness of an MPPT-based dp/dv with PID feedback method is enhanced using FL optimized by the big bang–big crunch optimizer. A research work in [73] proposed a comparison between the MPPT dp/dv with PID feedback method, P&O, and IC, which confirmed the advancement of this technique in comparison to the other techniques. An advanced implementation of a nonlinear PID (NPID) regulator is suggested in [74] in order to achieve the MPP in a PV system. The designed NPID parameters are tuned via the teaching-learning-based optimizer.

In this paper, we propose a robust scheme to enhance the performance of a PV system. This scheme is mainly based on the designing of a fractional-order PID (FOPID) controller as the MPPT technique to quickly achieve the maximum power. The MPPT-based dp/dv feedback approach with a FOPID controller is incorporated to achieve the main objective. In order to tune the FOPID controller parameters, a novel aquila optimizer algorithm (AO) is introduced to optimize the FOPID controller gains. The simulation results with the

suggested AO-based FOPID controller are compared with those obtained with the moth flame optimizer (MFO). On the other hand, the performance of the FOPID-controller-based MPPT method is compared with the conventional P&O and classical PID approaches. The main contributions of this research work are as follows: (i) to enhance the MPPT of a PV system, an advanced FOPID controller is suggested and discussed in terms of the effectiveness of the MPPT, (ii) to suggest that FOPID is an adjustable controller, as it is capable of maintaining the simpleness of a classical PID regulator, (iii) The effectiveness of the FOPID regulator in terms of MPPT is discussed based on various rigorous and practical climatic profiles, and it surpasses other conventional MPPT algorithms, and (iv) for the first time in MPPT design, the regulator gains are accurately tuned utilizing the AO algorithm.

A qualitative comparative analysis of the abovementioned MPPT techniques is tabulated in Table 1. Moreover, this table is useful as a literature review in the future for precisely choosing a suitable MPPT approach.

Table 1. A qualitative comparative analysis of MPPT techniques.

MPPT Approach	Application	Complexity Level	Convergence Rapidity	Noticed Parameters	Preceding Training	Cost	Efficiency
P&O [12,16]	Stand-alone	Modest	Alternates	Current Voltage	None	Low	Up to 95%
IC [28,29]	Stand-alone	Intermediate	Alternates	Current Voltage	None	Low	Up to 97%
ANN [39–41]	Both	Advanced	Rapid	Relates	Yes	High	Up to 98%
FL [48,49]	Both	Advanced	Rapid	Relates	None	High	Up to 98%
SMC [25]	Both	Advanced	Rapid	Relates	None	High	Up to 98%
Optimization approaches [53–65]	Both	Advanced	Rapid	Relates	None	High	Up to 98%
Hybrid techniques [38,47,50]	Both	Advanced	Rapid	Relates	None	High	Up to 98%
dp/dv feedback-control-based PID [73]	Both	Intermediate	Rapid	Voltage Power	None	Medium	Up to 98%
dp/dv feedback-control-based NFOPID [75]	Both	Advanced	Rapid	Voltage Power	None	Medium	Up to 98%

The organization of this paper is divided as follows. An overview of solar energy sources, an introduction to the MPPT approach, and the state-of-the-art of MPPT techniques were discussed in Section 1. The formulation and modeling of the entire system is presented in Section 2. The overview of MPPT control with the suggested technique is exposed in Section 3. Section 4 illustrates the proposed novel optimization method. Section 5 announces the fitness function formulation. The analysis of the simulation results with their interpretation is discussed in Section 6. The robustness test and its relevant analysis are presented in Section 7. Finally, the paper is concluded by a general conclusion in Section 8.

2. PV System Modeling

The principal components of a PV system consist of a solar module, which includes the series-parallel connections of solar cells, and a DC–DC converter, which can be controlled by an MPPT regulator and the load. The modeling of a PV system is presented in the next sub-sections.

2.1. Modeling of PV Panel Single Diode Model

A PV cell with a single-diode model (SDM) is a simple and efficient model. The SDM is used to study the behavior of PV systems. The photocurrent source is connected in parallel with the diode and shunt resistor, respectively, and a series resistor is also attached to the aforementioned devices, as shown in Figure 1.

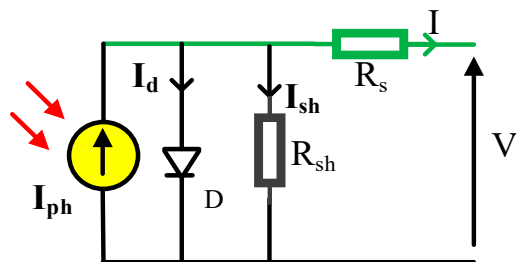


Figure 1. PV cell model of a single diode.

A PV panel has a number of PV cells of the same type, which are either connected in series to increase the voltage or in parallel to boost the current. The global current equation model is given in Equation (1) [76].

$$I = I_{ph}N_p - I_s N_p \left[\exp \left(\frac{q \left(\frac{V_{pv}}{N_s} + \frac{IR_s}{N_p} \right)}{AKT} \right) - 1 \right] - \left(\frac{\frac{VN_p}{N_s} + IR_s}{R_{sh}} \right) \quad (1)$$

where I_{ph} is the photocurrent. I_s represents the diode saturation current. R_s is the series resistor. R_{sh} is the parallel resistor. K denotes the Boltzmann constant ($1.3806503 \times 10^{-23}$). A is the diode ideality factor. q represents the electron charge ($1.6021764 \times 10^{-19}$). T is the temperature, in Kelvin, of the PV module in operation. N_s and N_p are the series and parallel numbers of PV cells connected together, respectively. V and I are the output of voltage and current, respectively, of the PV module.

In this study, a commercial M/S Kyocera type KC130GT PV panel is used, and its parameters are presented in Table 2.

Table 2. KC130GT module characteristics.

Parameter	Value
I_{ph} (A)	8.0428
I_s (A)	2.2655×10^{-10}
R_s (Ω)	0.22151
R_{sh} (Ω)	78.0854
A	0.97611
N_s	36
N_p	1

It should be noted that the parameter values showed in Table 2 were measured at the standard test conditions (STC) of 1000 W/m^2 of solar irradiation and a temperature of 25°C . However, the power–voltage P(V) and current–voltage I/V characteristics of the PV panel under variable climatic conditions of irradiation and temperature were realized ($1000, 500$, and 100 W/m^2 at 298 K (25°C) and $318, 308$, and 298 K at STC 1000 W/m^2), respectively, and Figure 2a,b present the I/V and P/V curves of the PV panel.

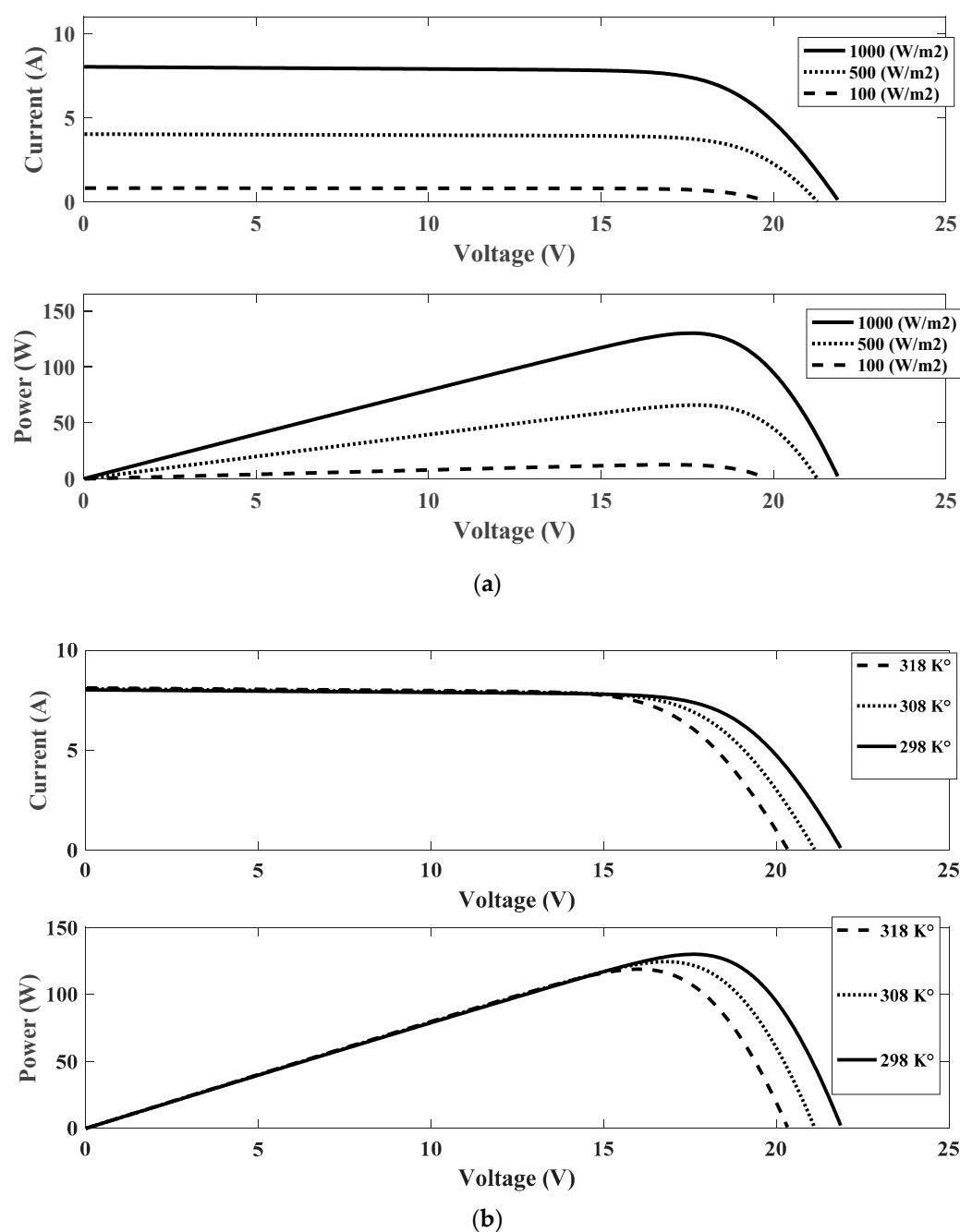


Figure 2. I-V and P-V characteristics of PV panel: (a) at variable irradiation conditions and (b) at variable temperature conditions.

2.2. DC/DC Converter

A DC/DC converter is a device that combines the PV generator and the load. This static converter represents a dynamic system because it contains switching devices (IGBT, MOSFET, etc.). The literature contains three configurations of DC/DC converters, namely boost, buck, and buck-boost. Therefore, the boost converter has fewer components compared to other DC/DC converters. It steps up the voltage and current to work at the MPP point [75]. Further, a boost converter is designed to track the MPP for all climatic conditions, especially under less irradiation. The boost converter configuration used in this study is presented in Figure 3.

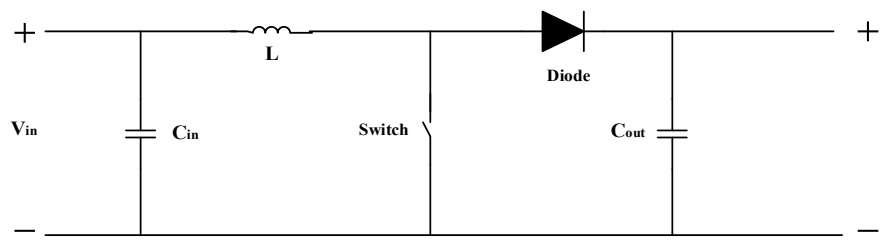


Figure 3. Boost converter configuration.

The relationship between the inputs and outputs of the electrical parameters is given in Equation (2).

$$V_{out} = \frac{V_{in}}{1-d} \quad (2)$$

where V_{in} and V_{out} are the input and output voltages of the PV system, respectively. I_{in} and I_{out} represent the input and output current of the PV system, respectively. d is the duty cycle parameter.

As can be observed from Equation (2), the relationship between the input and output of the PV system is dependent on the duty cycle values. For this reason, the PV system needs an MPPT controller to manage the PV system process. The next section explains the MPPT control techniques.

3. MPPT Control

The MPPT control process is an essential part of the PV system chain. It generates an adequate variable duty cycle, which pulses the switch of the DC/DC converter using a pulse width modulation (PWM) generator. This MPPT control forces the PV system to work at the maximum power point. In this study, the conventional perturb and observe (P&O) technique is implemented. The dp/dv feedback-based PID and FOPID controllers are demonstrated in the following step [77].

3.1. MPPT dp/dv Feedback Method-Based Controller

The derivative dp/dv represents the slope of the P-V curve. Otherwise, it can be clearly seen that the MPP is at the summit of the P-V curve when the slope of dp/dv is equal to zero. In the proposed method, $dp/dv = 0$ is set as a reference for the MPPT controller. Figure 4 represents the block diagram of the dp/dv MPPT control to calculate the slope of dp/dv and compare it with a set reference point of zero. The resulting value of the error is treated by the control process, which generates the duty cycle sequences to supply the DC/DC converter switch gate [70].

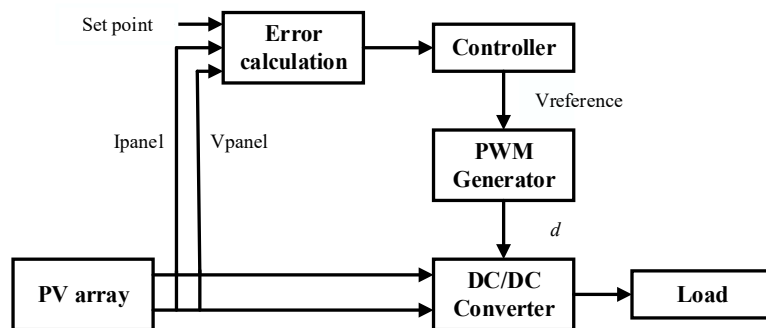


Figure 4. dp/dv feedback-based MPPT monitoring diagram.

It can be seen from Figure 4 that the controller input is the error value, and it represents the dp/dv slope, which is actuated by the feedback mechanism of the PV system. Hence, the controller generates an output voltage as a control signal (duty cycle variation) to

the DC/DC converter switch through the PWM generator. In this study, the proposed fractional order PID (FOPID) controller with a classical PID controller is described in the following sub-section.

3.2. Fractional Calculus

Conventional calculus addresses integrals and derivatives owning an integer order (d/dx , d^2/dx^2). Leibniz and L' Hopital suggested the employment of fractional calculus theory instead of conventional calculus theory. Consequently, several mathematicians contributed to the development of fractional calculus theory. In the control systems domain, the fractional calculus process has been widely applied, in which fractional-order integration and differentiation can be utilized in the concept of a regulator. Through distributed and variable-order functions, it simplifies standard integer-order calculus. In recent years, and, according to their effectiveness towards system gain changes and system uncertainties, fractional regulators have been extensively employed. Their conceptual requirements of gain and phase margins should be smoothly tuned via FO controllers comparatively to integer-order controllers. Several parameters are included in FO controllers in comparison to integer-order controllers. This specified design should be fulfilled [78].

3.3. PID Controller Description

The parallel combination of three control effects, which are the proportional (P), integral (I), and derivative (D) gains, form the conventional PID controller. Further, the principle of this controller is based on the feedback chain in order to calculate the error value. This error calculation continues during the operating loop and under any irradiation and temperature changes. The error value in this is the dp/dv slope, which must be equal to zero to track and achieve the MPP at the top of the P(V) curve. Thus, the signal generated by the PID controller through the controlling loop that maintains the operating system oscillates around the MPP. The mathematical formulation of the PID controller is shown in the following equation:

$$p_{PID}(t) = K_p e(t) + K_i \int e(t) + K_d \frac{de(t)}{dt} \quad (3)$$

where K_p , K_i , and K_d are the proportional, the integral, and the derivative gains, respectively.

3.4. Proposed Fractional-Order PID Controller

To improve the effectiveness of PID controller design, Podlubny suggested an expansion to PID controllers, which is named FOPID. This controller involves the differentiator and integrator of μ and λ and is detailed in [79]. The definition of the Riemann–Liouville (RL) function is applied to the design of the fractional differ-integral, which is described as follows:

$$\alpha D_t^\alpha F(t) = \frac{1}{\Gamma(n-\alpha)} \left(\frac{d}{dt} \right)^n \int_\alpha^t \frac{f(\tau)}{(t-\tau)^{1-(n-\alpha)}} d\tau \quad (4)$$

where Γ presents Euler's gamma function that defines the factorial and specifies the operator to obtain the value of a non-integer. The mathematical description of Grunwald–Letnikov function based on the definition of fractional differentiation is given as:

$$\alpha D_t^\alpha F(t) = \lim_{g \rightarrow 0} \frac{\Gamma(\alpha+d)}{\Gamma(g+1)} f(t-dg) \quad (5)$$

It is necessary to note that the integrator can be consolidated by applying the design of a fractional-order operator.

The transfer function of FOPID is attained by using the Laplace transform and is described as:

$$G_c(s) = K_p + K_i s^{-\lambda} + K_d s^\mu \quad (6)$$

The next equation illustrates the differential equation of a FOPID controller:

$$u(t) = K_p e(t) + K_i D_t^{-\lambda} e(t) + K_d D_t^{\mu} e(t) \quad (7)$$

The concept of a FOPID controller is based on the structure of the K_p , K_i , K_d , μ , and λ parameters. μ and λ are the derivative and integral factors, respectively. A FOPID controller has superior performance in terms of control system tuning (see Figure 5).

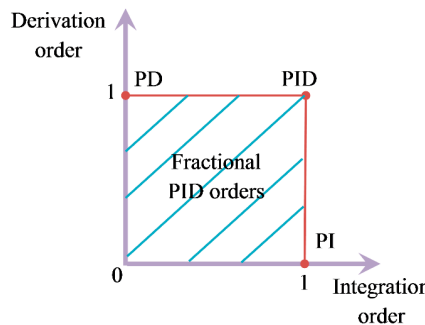


Figure 5. Fractional-order PID form.

4. Aquila Optimizer

In this work, we propose a meta-heuristic optimization algorithm called AO, which is inspired from nature by the behavior of an eagle during the procedure of hunting its target. The eagle represents one of the main common aggressive birds [79,80].

The optimization processes of the proposed method are divided into four main steps:

- Choosing the search boundary by elevated soaring and perpendicular stoop.
- Exploring within a diverged search boundary by a contour flight with a low glide swoop.
- Exploiting within a converged search boundary by a short flight with a slow drop swoop and swooping by walking and snatching the target.

In the following parts, the mathematical modeling of the AO algorithm is described.

4.1. Solution Initialization

AO is a population-based algorithm. The process of optimization starts by a population of a defined solution (X), as formulated in Equation (8), which is obtained stochastically through the maximum limit and minimum limit of the mentioned problem. The achieved superior solution is considered to be the best solution in nearly each generation.

$$X = \begin{bmatrix} x_{1,1} & \dots & x_{1,j} & x_{1,Dim-1} & x_{1,Dim} \\ x_{2,1} & \dots & x_{2,j} & \dots & x_{2,Dim} \\ \vdots & \vdots & \vdots & \vdots & \vdots \\ x_{N-1,1} & \dots & x_{N-1,j} & \dots & x_{N-1,Dim} \\ x_{N,1} & \dots & x_{N,j} & x_{N,Dim-1} & x_{N,Dim} \end{bmatrix} \quad (8)$$

where X is the set of actual defined solutions and is obtained randomly via Equation (9). X_i represents the i th solution's position. N denotes the maximum number of populations, and Dim is the mentioned problem's dimension space.

$$X_{ij} = rand \times (UB_j - LB_j) + LB_j, \forall i \in N \&& j \in Dim \quad (9)$$

where $rand$ is a value between 0 and 1. LB_j represents the j th minimum limit, and UB_j represents the j th maximum limit of the mentioned problem.

4.2. Mathematical Formulation of AO

As expressed before, the AO algorithm process has four global main steps. The transfer between the exploration phases and exploitation phases in the AO algorithm can be attained through several behaviors based on the instruction of if $t \leq (\frac{2}{3}) \times T$, then the exploration phases will be activated. Furthermore, the exploitation phases will then be calculated. The principal mathematical model of the four main steps in the AO algorithm is given as follows:

- **Step 1: Expanded Exploration (X_1)**

The eagle in this first step identifies the target region and chooses the best catching region by elevated soaring and performing a perpendicular stoop. In this step, AO commonly explores elevated soaring to define the region of the search boundary. Figure 6 illustrates the behavior of the eagle in the case of elevated soaring and the perpendicular stoop process, which is expressed in Equation (10).

$$X_1(t+1) = X_{best}(t) \times \left(1 - \frac{t}{T}\right) + (X_M(t) - X_{best}(t)) \times rand \quad (10)$$

where $X_1(t+1)$ represents the solution of the following generation of t , which is produced by the first search step (X_1). $X_{best}(t)$ is the superior achieved solution of the i th generation. To supervise the expanded exploration, the equation of $(1 - \frac{t}{T})$ is utilized by the applied iterations value. X_M is the mean value of the location in the actual solution according to the i th generation, which is obtained through Equation (11). $rand$ represents a random number. t is the actual generation, while T is the total number of generations.

$$X_M(t) = \frac{1}{N} \sum_{i=1}^N X_i(t), \forall j \in Dim \quad (11)$$

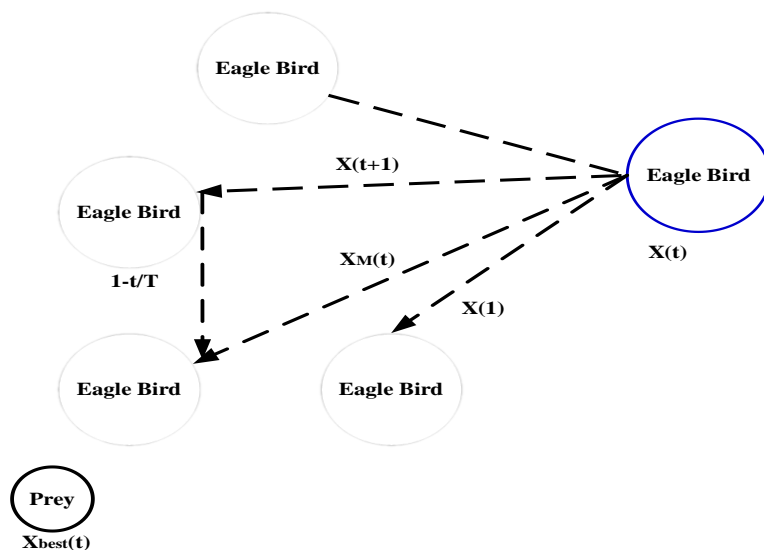


Figure 6. The behavior of the eagle in elevated soaring and the perpendicular stoop process.

- **Step 2: Narrowed Exploration (X_2)**

In this step, in case of preparation for an attack, AO closely explores the chosen region of the target. Figure 7 presents the behavior of the eagle in a contour flight with a low glide swoop. This behavior is formulated as per Equation (12):

$$X_2(t+1) = X_{best}(t) \times Levy(D) + X_R(t) + (y - x) \times rand \quad (12)$$

where $X_2(t+1)$ denotes the following generation solution of t . This solution is produced using the second step (X_2). X_R denotes a random solution between 1 and N at the i th generation. D represents the dimension search size, and $\text{Levy}(D)$ denotes the function of the levy flight division, which is given in Equation (13):

$$\text{Levy}(D) = s \times \frac{u \times \sigma}{|\nu|^{\frac{1}{\beta}}} \quad (13)$$

where u and v represent a random value taken in the range $[0, 1]$. s denotes a fixed value of 0.01. σ is variable value formulated in Equation (14):

$$\sigma = \left(\frac{\Gamma(1 + \beta) \times \sin\left(\frac{\pi\beta}{2}\right)}{\Gamma\left(\frac{1+\beta}{2}\right) \times \beta \times 2^{\left(\frac{\beta-1}{2}\right)}} \right) \quad (14)$$

where β denotes a fixed value of 1.5. y and x are calculated using Equations (15) and (16) and are used to show the spiral form during the process of searching. These latter values are found below.

$$y = r\cos(\theta) \quad (15)$$

$$x = r\sin(\theta) \quad (16)$$

where:

$$r = r_1 + UD_1 \quad (17)$$

$$\theta = -\omega D_1 + \theta_1 \quad (18)$$

$$\theta_1 = \frac{3\pi}{2} \quad (19)$$

where r_1 is a selected value from 1 to 20 during the search cycles. U takes a value of 0.00565. D_1 represents the numbers of an integer between 1 and $\text{length}(\text{Dim})$, and ω takes a value of 0.005. Figure 8 illustrates the behavior of AO in a spiral form.

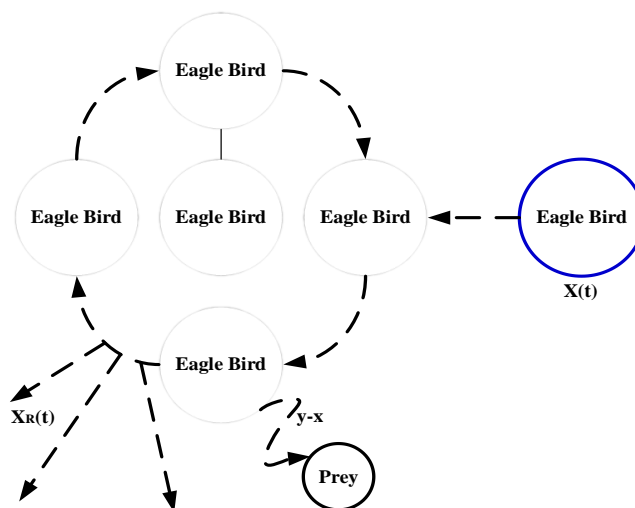


Figure 7. The behavior of the eagle in the process of contour flight with low glide swoop.

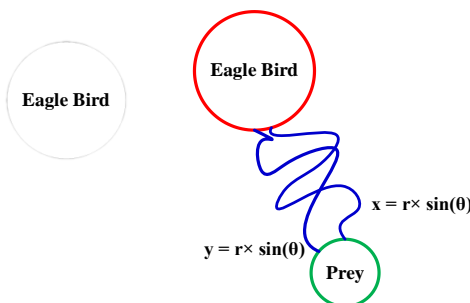


Figure 8. The behavior of the eagle in a spiral form.

- **Step 3: Expanded Exploitation (X_3)**

In this step, in the case of getting close to attacking, AO exploits the chosen region of the prey, which is expressed in Equation (20):

$$X_3(t+1) = (X_{best}(t) - X_M(t)) \times \alpha - rand + ((UB - LB) \times rand + LB) \times \delta \quad (20)$$

where $X_3(t+1)$ represents the solution of the following generation of t , which is produced by the third search step (X_3). $X_{best}(t)$ is the superior achieved solution of the i th generation. X_M is the mean value of the location in the actual solution according to the i th generation, which is obtained through Equation (11). $rand$ represents a random number. α and δ present the attained parameters of exploitation, which are selected as 0.1.

- **Step 4: Narrowed Exploitation (X_4)**

In this final step, in the case of the last location, AO hunts the target, which is expressed in Equation (21):

$$X_4(t+1) = QF \times X_{best}(t) - (G_1 \times X(t) \times rand) - G_2 \times Levy(D) + rand \times G_1 \quad (21)$$

where $X_4(t+1)$ represents the solution of the following generation of t , which is produced by the fourth search step (X_4). $X_{best}(t)$ is the superior achieved solution of the i th generation. $QF(t)$ is formulated using Equation (22), which presents the function of quality applied to balance the search organization. G_1 is calculated using Equation (23), which presents different movements of the algorithm that are employed to follow the target through the escape. G_2 is generated using Equation (24), which denotes a diminishing from 2 to 0 that is employed to follow the target through the escape from the initial position (1) to the final position (t). $X(t)$ is the actual defined solution at the i th generation.

$$QF(t) = t^{\frac{2 \times rand - 1}{(1-T)^2}} \quad (22)$$

$$G_1 = 2 \times rand - 1 \quad (23)$$

$$G_2 = 2 \times \left(1 - \frac{t}{T}\right) \quad (24)$$

where $QF(t)$ denotes the value of a quality function at the i th generation. $rand$ represents the value of a random variable fixed in the range of $[0, 1]$, t is the actual generation, while T is the total number of generations. $Levy(D)$ denotes the function of the levy flight division, which is given in Equation (13).

5. Fitness Function Formulation

The problem of the adjustment of the parameters of controller gains haWe revise it, please confirs become a big task for scientific researchers because of the fact that there are a lot of techniques that exist in the literature. Each technique has its own specifications and

calculation parameters. Lastly, the optimization techniques play a significant role in the parameter tuning of these controllers. A novel proposed AO algorithm was selected in this study for this adjustment.

The tuning of the FOPID controller gains (K_p , K_i , K_d , μ , and λ) is achieved using the AO algorithm. The fitness function was chosen as the integral of the time-weighted absolute error (ITAE). The ITAE heavily penalizes errors during the simulation time to obligate the system to track the exact global MPP [74]. Thus, the fitness function formulation is given in Equation (25):

$$\text{Fitness_value} = \sum_{n=1}^N \left(\left| 0 - \frac{dP}{dV} \right| (nt)(t) \right) \quad (25)$$

where nt is a time parameter and t indicates the sample time. The flowchart shown in Figure 9 represents the optimization process.

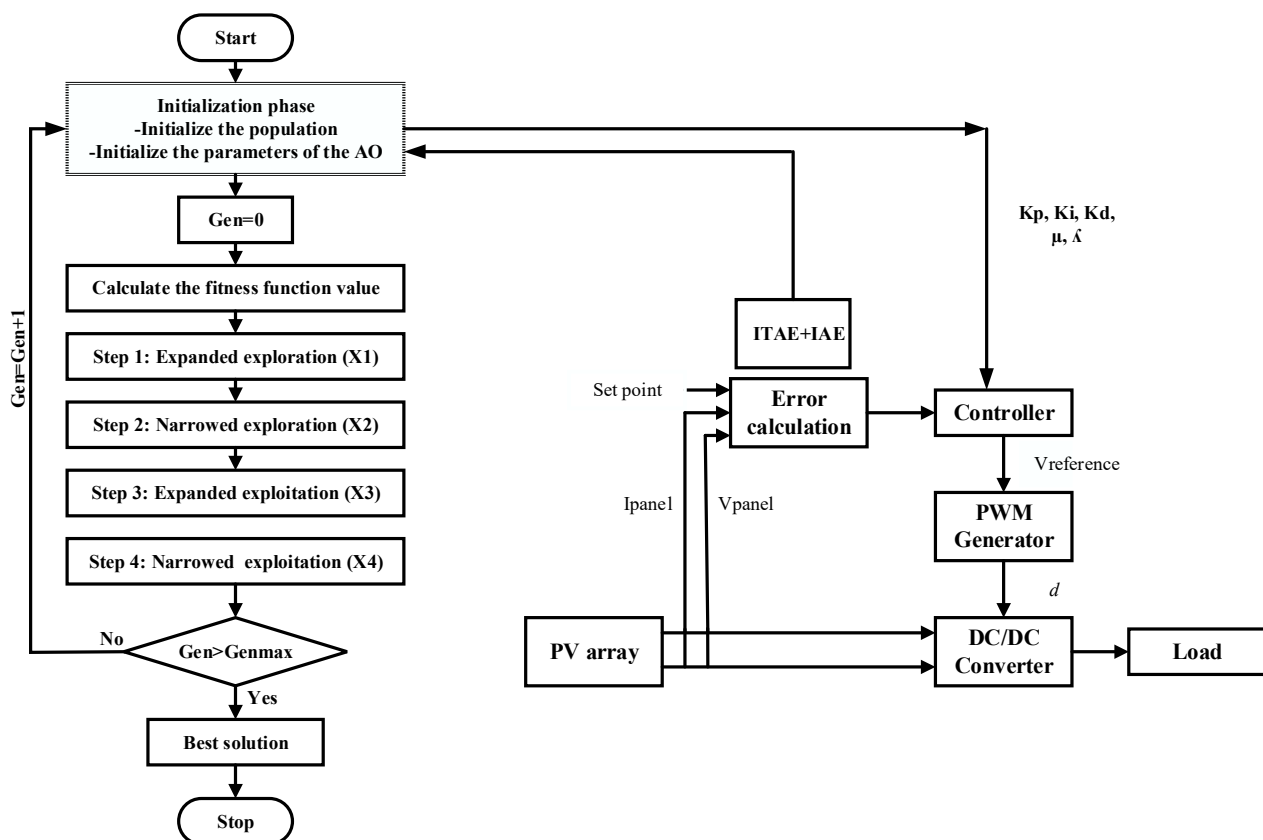


Figure 9. Organigram for tuning of FOPID and PID parameters using AO.

The best set gains obtained by the FOPID controller are attained and further integrated into the PV system process in order to lead the system's response towards a steady state. Therefore, the fitness function value should be at the minimum value to keep the PV system continuously tracking the MPP. The standard conditions of irradiation and temperature of 1000 W/m^2 and 25°C are fixed during the tuning phase, while the computation of the fitness value is accomplished for 0.005 s . Thus, in this study, the calculation process was performed in the environment of MATLAB 2016b with a held sample time of $10 \mu\text{s}$.

In the tuning step, both the FOPID and PID controllers were tuned by the proposed AO algorithm, but the difference between them was the gains number. The higher and lower bound limits of the two tuned FOPID and PID controllers are presented in Table 3.

Table 3. The bound limits for FOPID and PID controllers.

FOPID Parameter	PID Parameter	Lower Range	Higher Range
K_p	K_p	0.001	100
K_i	K_i	0.001	100
K_d	K_d	0.001	100
μ	-	0.100	0.95
λ	-	0.1	0.95

6. Simulation Results and Discussion

In this part, we conducted a comparative study between the proposed FOPID and PID controllers and a P&O-based MPPT classical technique. The robustness of our controller tuning was assessed by evaluating MPP tracking under various irradiation and temperature values. In addition, it was preferable to verify the response speed of the presented controller's tuning process under changing climate conditions. Thus, to validate the effectiveness of our method, we studied several environmental profiles of operating conditions, including daytime and sinusoidal scenarios. Hence, in order to evaluate the efficiency of the system's response, all the mentioned profiles were captured in various proportions for the attained system signals in both transient and steady-state responses. Furthermore, we included transient increase and decrease periods in the power curve. The MPPT controller needed a short time to achieve the maximum power level for the transition period within a suitable band. Additionally, because of the oscillatory behavior of the MPPT controllers after attaining the MPP during the transition period, error criteria were calculated to evaluate the system's response at the reached MPP. In this study, the total simulation time of all the environmental profiles was chosen as 1 s in order to interpret the daytime performance with a scaling of 12 h.

The best achieved parameters of the proposed controller are presented in Tables 4 and 5. Figure 10 shows the fitness value versus the generation plot of the AO and MFO algorithms. In addition, Figure 11 illustrates the fitness value versus the generation plot of the FOPID and PID controllers. It can be seen from these figures that the proposed algorithm outperformed the MFO algorithm in terms of obtaining the minimum fitness value. Also, the convergence rate using AO appeared to be more rapid in comparison with MFO. Otherwise, the designed FOPID controller attained the best fitness value compared to PID, which proves the superiority of FOPID in terms of the control signal.

Table 4. Best parameters of FOPID tuned by AO and MFO.

Controller	Proposed Algorithms	K_p	K_i	K_d	μ	λ	Fitness Value
FOPD	AO	69.6734	100.0000	0.0010	0.6398	0.5502	0.0179
	MFO	25.3656	99.9312	15.8049	0.5809	0.1000	0.0185

Table 5. FOPID and PID controller parameters tuned using proposed algorithms.

Proposed Algorithms	Controllers	K_p	K_i	K_d	μ	λ	Fitness Value
AO	FOPID	69.6734	100	0.0010	0.6398	0.5502	0.0179
	PID	93.0756	100	0.0010	-	-	0.0186

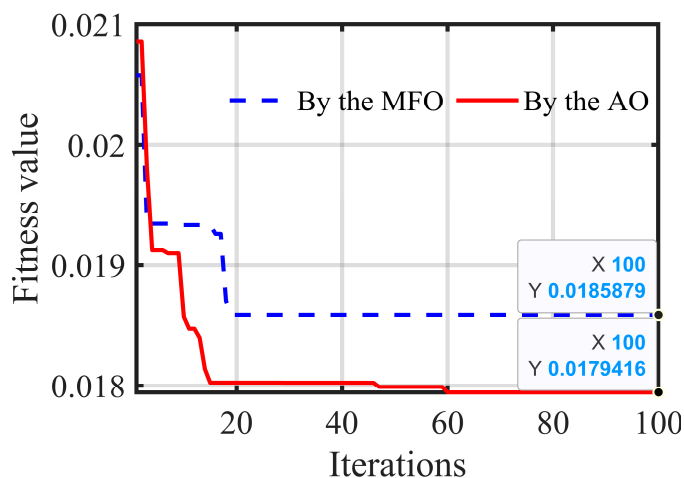


Figure 10. Convergence curves of fitness value using AO and MFO.

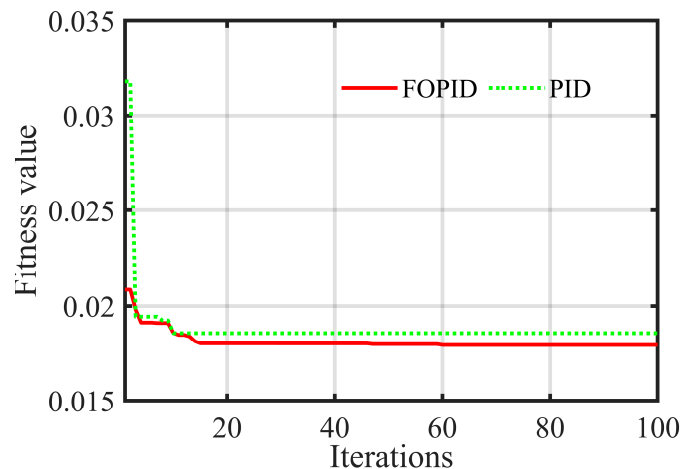


Figure 11. Convergence curves of fitness value for FOPID and PID controllers.

6.1. MPPT Controller Performance Tests

Under uniform climate conditions, MPPT controllers offer an elevated response efficiency. Otherwise, to confirm the robustness of the proposed controller, we tested it under various irradiation and temperature levels. Furthermore, the evaluation of the system's responses under quick environmental changes was required. In this sub-section, a quick variation in the irradiation profile was applied while fixing the temperature at STC (25°C) and vice versa.

6.1.1. Irradiation Variation for Daytime Profile

Figure 12a represents the test profile of the variable irradiation between a lower value of 600 W/m^2 and an upper value of 1000 W/m^2 . During this irradiation profile, the temperature was fixed at the level of 25°C .

The achieved output power results are shown in Figure 12b. It was rapidly observed that the classical MPPT controller was less effective than the proposed controller under the lower irradiation values. In addition, in order to analyze the power evaluation during a daytime profile, four zones are presented (1, 2, 3, and 4), which reflect the progression of rising and dropping. The proposed MPPT techniques were evaluated at each zone of the power profile. The mentioned zones present the captured power, which describes the system performance of the MPPT controllers at the mentioned zones. Hence, in order to

investigate the schematic and numerical forms, the attained system responses are denoted for the comparison of their effectiveness.

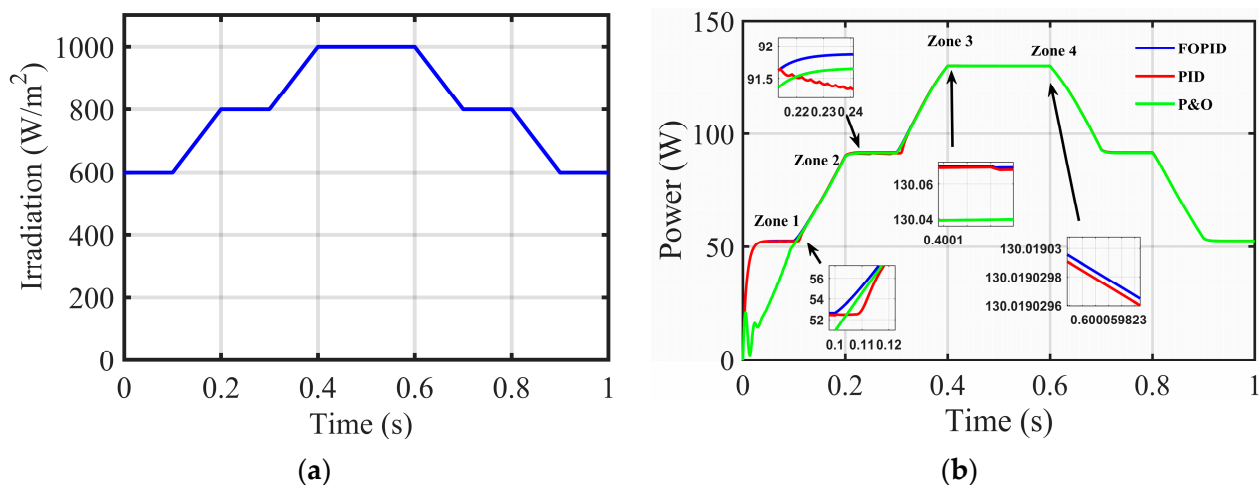


Figure 12. Performance during daytime irradiation profile. (a) Irradiation variation for daytime profile. (b) Power response.

The four zones (1, 2, 3, and 4) presented in Figure 12b showed a rise and a drop in the power amount at the mentioned zones. In addition, Table 6 depicts the results of the performance index (PI) under the daytime irradiation profile. It can be obviously seen that the studied FOPID controller gave a low overshoot value compared with the PID and P&O-based MPPT techniques. In addition, as can be seen from the power curves of zones 2 and 3, a rise in the irradiation level was accompanied by an increased power level. In this case, all the MPPT techniques had unstable behaviors during the tracking of the MPP except for the proposed FOPID controller, which kept the power tracking stable during this transient part. The effect of the parameters on the proposed FOPID always obligated the process to follow the set point. At zone 4, a decrease in the power level due to a drop in the irradiation amount was noticed. The robustness of the proposed controller was attained compared with the other controllers based on MPPT.

Table 6. Results of PI under daytime irradiation profile.

PI	Zone	FOPID	PID	P&O
Overshoot (W)	1	-	-	-
	2	2.9346×10^{-4}	0.1486	2.1457×10^{-3}
	3	0.0031	0.0040	0.0044
	4	0.0147	0.0147	0.0180

6.1.2. Irradiation Variation for Sinusoidal Profile

Because of the linearity of the previous daytime profile and in order to test the proposed method under non-uniform irradiation, the following test profile contained a non-linear signal, which was the sinusoidal scenario. Figure 13a shows the sinusoidal profile test with the irradiation changing between 900 W/m² and 1000 W/m². In addition, the operating temperature was kept at 25 °C (STC) during this profile test.

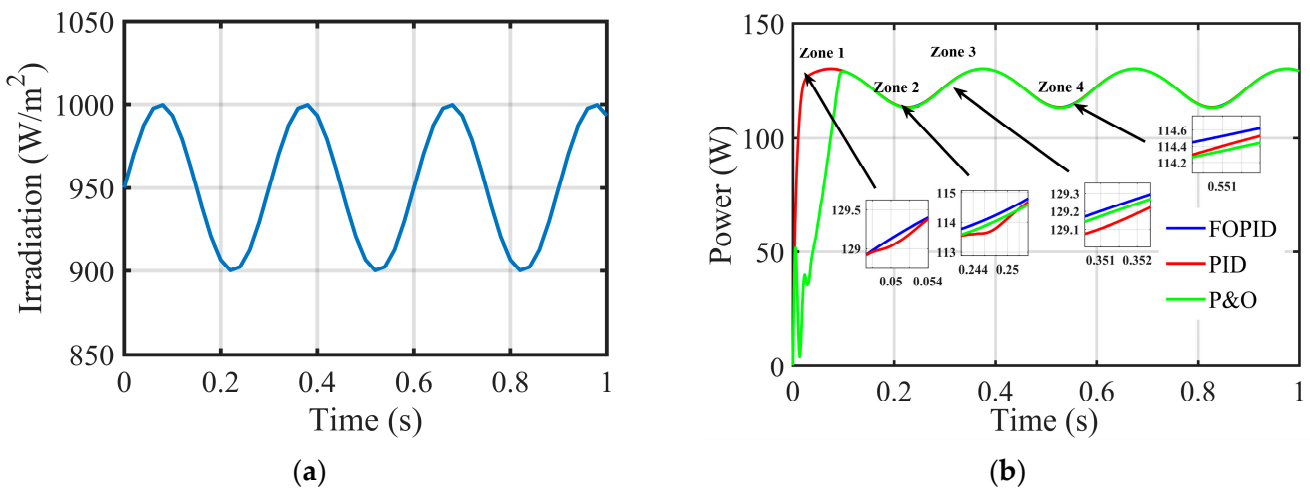


Figure 13. Performance during sinusoidal irradiation scenario. (a) Irradiation changing for sinusoidal profile. (b) Power response.

Figure 13b presents the output response during the sinusoidal irradiation scenario test. The results of the PI under the sinusoidal irradiation profile are shown in Table 7. Clearly, the system response had no unexpected changes according to the smooth irradiation changes. Furthermore, in order to examine the system response performance, four test zones were involved in this scenario, which were 1, 2, 3, and 4, in order to evaluate the system responses for all the MPPT techniques.

Table 7. Results of PI under sinusoidal irradiation profile.

PI	FOPID	PID	P&O
Overshoot (W)	4.5088×10^{-4}	5.0118×10^{-4}	Out of zone

The four zones (1, 2, 3, and 4) shown in Figure 13b denote the enlarged responses for the three MPPT techniques. Hence, in order to investigate the schematic and numerical forms, the achieved system responses are shown with comparisons of their effectiveness. From these zones, it can be observed that the suggested FOPID controller obtained a lower overshoot in contrast to the other MPPT techniques. The proposed FOPID was able to adapt to environmental variations and presented a minimum divergence from its planned power position, which proves its advancement compared with the other techniques.

6.1.3. Temperature Variation for Daytime Profile

In this test profile, the temperature bounds were taken as the real magnitude of the desert area in the south of Algeria between a lower level of 30 °C and a higher level of 48 °C. Furthermore, the irradiation value was kept at 1000 W/m² (STC) during the present temperature test profile. Figure 14a shows the daytime temperature profile used in this part of the work.

The three zones (1, 2, and 3) shown in Figure 14b present the power responses of the temperature variation for the daytime profile. As mentioned, the changes in the temperature did not result in severe variations in the system behavior in contrast with the changes in the irradiation. In addition, the system behavior was examined at the three test zones, which were zones 1, 2, and 3, respectively. It can be observed that the suggested FOPID controller at zones 1 and 3 gave the minimum undershoot compared to the other controllers based on MPPT. Zone 1 was located in the transient period with a rise in the system response. Otherwise, zone 3 presented a stable system response due to the temperature change.

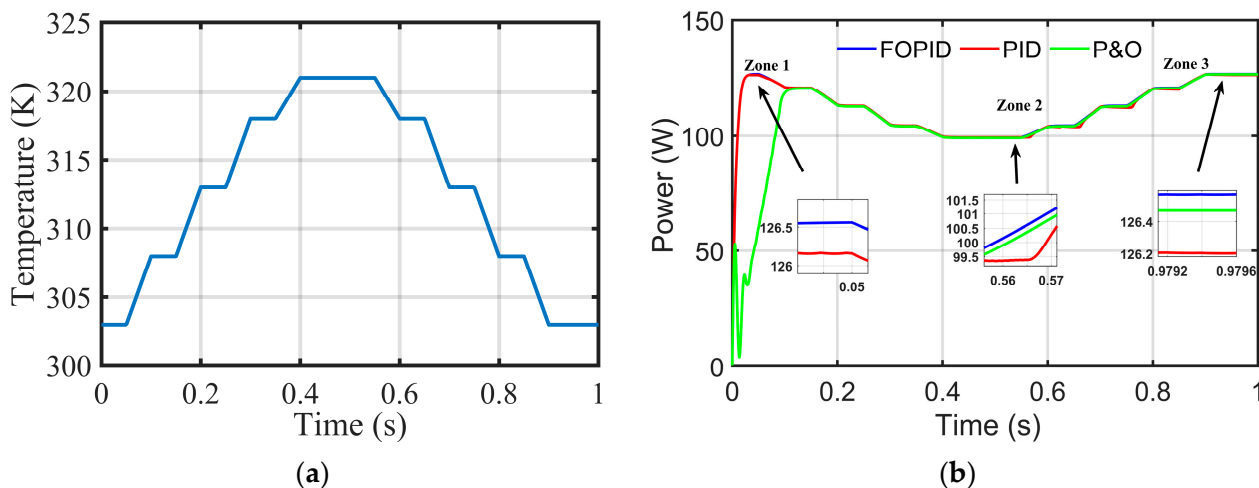


Figure 14. Performance during daytime temperature profile. (a) Temperature variation for daytime profile. (b) System responses.

Table 8 denotes a comparison of the PI of the three controllers. As noted, the PI value presented minimum variations in contrast to the daytime profile of the variation in the irradiation. From this table, these results again confirmed the capability of the FOPID controller to accurately attain the MPP under varying temperature conditions in terms of the daytime profile compared to the other MPPT-based controllers.

Table 8. Results of PI during daytime temperature profile.

PI	FOPID	PID	P&O
Overshoot (W)	2.3340	2.5665	Out of zone

6.1.4. Temperature Variation for Sinusoidal Profile

The sinusoidal profile test is presented in Figure 15a. The evolution of the temperature signal test was fixed between the lower and higher values of 20 °C and 48 °C, respectively. During the applied temperature profile test, the irradiation value was kept constant at 1000 W/m² (STC).

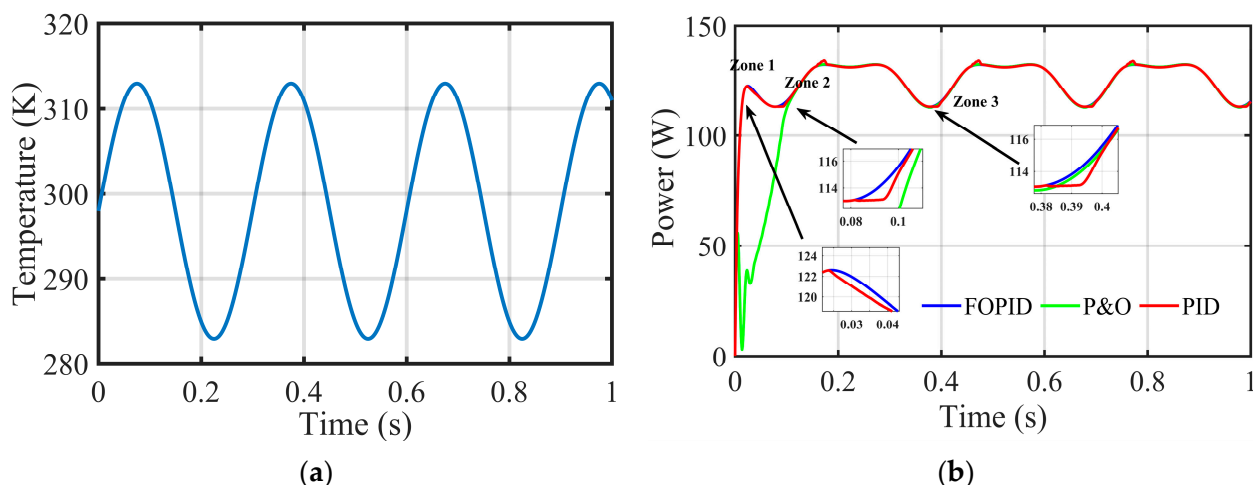


Figure 15. Performance during sinusoidal temperature profile. (a) Temperature variation for sinusoidal profile. (b) System responses.

Figure 15b presents the output power response obtained during the sinusoidal temperature profile. To confirm the robustness of the system response, three zones (1, 2, and 3) were chosen in this part for all the MPPT-based controllers. Table 9 presents the PI of the output system responses attained with the applied controllers during the sinusoidal temperature profile. The zones 1, 2, and 3 denote the enlarged responses obtained with the three MPPT controllers. The achieved system responses are shown with comparisons of their effectiveness.

Table 9. Results of PI during sinusoidal temperature profile.

PI	FOPID	PID	P&O
Overshoot (W)	5.0186	5.0980	Out of zone

Additionally, it can be noted from these figures that the suggested FOPID controller ensured a lower ripple compartment compared to the other MPPT controllers. Nevertheless, it is clear to say that the behavior of the FOPID controller's response presented a better performance compared to the PID controller in the case of the sinusoidal temperature profile. It was noted that the temperature changes had a lesser effect on the system response in contrast to the variation in the irradiation. As mentioned above, zone 1 depicts the top of the response allure, while zones 2 and 3 illustrate the bottom of the response allure. The proposed FOPID controller had better performance indices compared to the other competitive controllers.

7. Robustness Test

Load Variation

A test simulation was conducted to evaluate the performance of the PV array and the implemented MPPT control system under varying loads. During the execution phase, the resistive load was connected to the boost converter terminal. Load variations were tested in conjunction with irradiance variations following a daytime profile. This scenario was chosen due to the significant impact of irradiance changes on the output power compared to temperature changes. To assess the impact of load fluctuations on the PV system's performance, the load was separately increased and decreased by 10% of its nominal value. This test effectively evaluated the performance of the proposed controllers. Figures 16 and 17 illustrate the output power response to the load variations with the proposed controllers. From the captured zones (1, 2, and 3), the results clearly demonstrated that the suggested controller maintained its reputation and exhibited a robust performance in response to the load variations, efficiently tracking the MPP. Additionally, the FOPID controller demonstrated its capability to track the MPP with minimal power losses when compared to the other controllers.

Performance Indices Test

To facilitate a more comprehensive comparison and assess the effectiveness of each proposed controller design, various performance indices related to the system output power were utilized and are presented in Table 10 for each controller.

From the performance indices presented in this table, it became evident that the FOPID controller consistently yielded the lowest error across the various functions and scenarios when compared to both the PID and P&O techniques. This superiority can be attributed to the higher emphasis placed on minimizing both the error and time in the optimization criteria, validating the efficacy of the proposed controller. Furthermore, it is clear that the FOPID controller consistently demonstrated the lowest control costs in all cases, outperforming all the other controllers in this aspect.

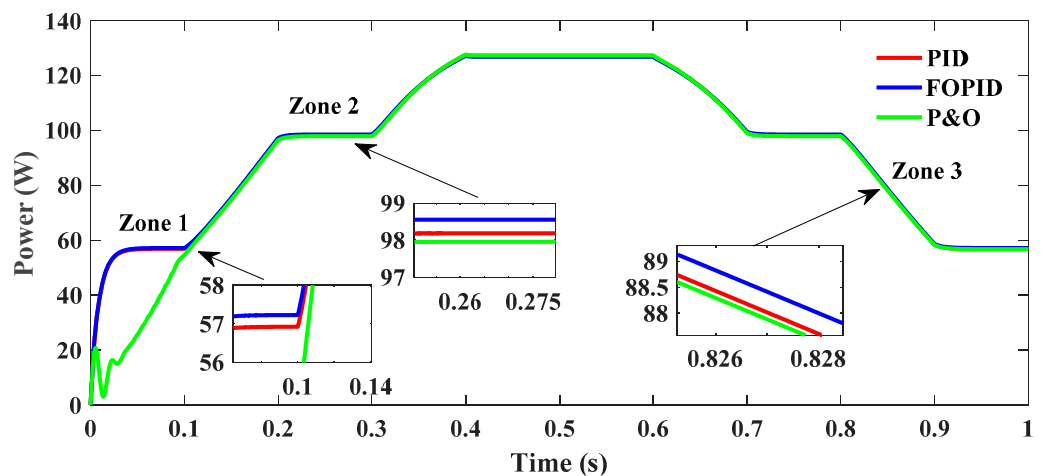


Figure 16. Output power response under load variations of +10%.

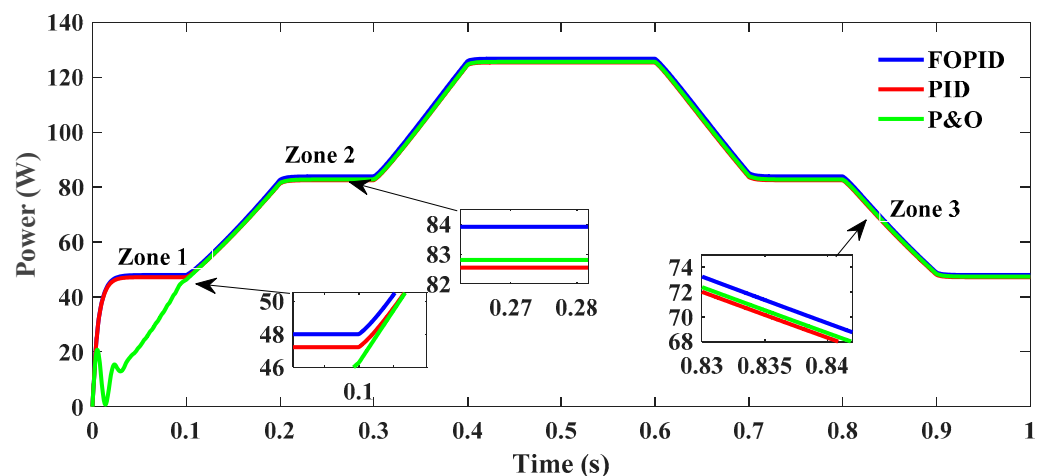


Figure 17. Output power response under load variations of -10%.

Table 10. Performance indices values with different proposed controllers.

Controllers	ISE	IAE	ITSE	ITAE
Irradiation variation for daytime profile	P&O	0.0101	0.0283	0.0026
	PID	0.0264	0.0452	0.0068
	FOPID	0.0015	0.0109	3.8856×10^{-4}
Temperature variation for daytime profile	P&O	0.0028	0.0110	0.0017
	PID	0.0061	0.0169	0.0038
	FOPID	3.3339×10^{-4}	0.0035	2.0605×10^{-4}

8. Conclusions

In this study, a new AO algorithm was applied to tune the suggested MPPT-based controllers. A PV solar module associated with a boost converter was utilized. A robust FOPID controller was investigated based on fractional calculus to extract the maximum power. The FOPID controller parameters were optimally attained using the AO algorithm. To test the robustness of the proposed controller, we tested it in large simulation scenarios of climatic profiles, including irradiation and temperature variations with various periods of rising, steady-state, and dropping patterns. The output system responses were evaluated by the use of a performance index. The ITAE was carried out as a fitness function to

optimize the controller parameters and demonstrate the performance of the proposed scheme. The simulation results proved that the suggested FOPID controller better adapted to the fluctuation generated compared to the classical PID controller and P&O techniques. The proposed algorithm achieved the minimum fitness value. Also, the AO algorithm converged more rapidly compared to the MFO algorithm. Our proposed FOPID controller tuned by AO showed superiority for all the tested scenarios of irradiation and temperature variations and provided a high efficiency in the tested PV system.

Author Contributions: Conceptualization, M.T. and L.C.; Methodology, M.T. and L.C.; Software, M.T. and A.C.; Validation, L.C., A.C., A.-M.A., A.F., H.R., M.L. and A.E.-F.; Formal analysis, M.T., A.C., A.-M.A., A.F., H.R., M.L. and A.E.-F.; Investigation, M.T., L.C., A.C., A.-M.A., A.F., H.R., M.L. and A.E.-F.; Resources, M.T., A.-M.A., A.F., H.R. and A.E.-F.; Data curation, M.T., L.C., A.C., H.R. and A.E.-F.; Writing—original draft, M.T.; Writing—review & editing, M.T., L.C., A.C., A.-M.A., A.F., H.R., M.L. and A.E.-F.; Visualization, M.T., L.C., A.C., A.-M.A., A.F. and H.R.; Supervision, L.C., A.C., A.-M.A. and A.E.-F.; Project administration, A.F., H.R. and A.E.-F.; Funding acquisition, H.R., M.L. and A.E.-F. All authors have read and agreed to the published version of the manuscript.

Funding: This study was supported via funding from Prince Sattam bin Abdulaziz University, project number (PSAU/2023/R/1445).

Conflicts of Interest: All authors agreed to contribute to the paper, and the authors declare that they have no known competing financial interests or personal relationships that could have appeared to influence the work reported in this paper. We declare that no-one participated in the preparation of the manuscript, nor did they qualify for authorship.

Nomenclature

Variables	Abbreviations
μ	Differentiator of order
λ	Integrator of order
I_{ph}	Photocurrent
I_s	Diode saturation current
R_s	Series resistor
R_{sh}	Parallel resistor
K	Boltzmann constant
A	Diode ideality factor
q	Electron charge
T	Temperature in Kelvin
N_s	Series number of PV cells
N_p	Parallel number of PV cells
V	Output voltage
I	Output current
V_{in}	Input PV system voltage
V_{out}	output PV system voltage
d	Duty cycle parameter
K_p	Proportional gain
K_i	Integral gain
K_d	Derivative gain
Γ	Euler's gamma function
X	Population of defined solution
X_i	i th solution position
N	Maximum number of populations
	MPP Maximum power point
	PV Photovoltaic
	PID Proportional integral derivative
	FOPID Fractional order proportional integral derivative
	AO Aquila optimizer
	MFO Moth flame optimizer
	P&O Perturb and observe
	DC Direct current
	IC Incremental conductance
	FPA Flower pollination algorithm
	PSO Particle swarm optimizer
	LED Light-emitting diode
	ANN Artificial neural network
	STC Standard test conditions
	SMC Sliding mode controller
	FL Fuzzy logic
	NPID Nonlinear proportional integral derivative
	SDM Single-diode model
	IGBT Insulated gate bipolar transistor
	MOSFET Metal-oxide-semiconductor field-effect transistor
	ITAE Integral of time-weighted absolute error
	ISE Integral square error
	IAE Integral absolute error
	ITSE Integral time square error

<i>Dim</i>	Problem dimension space
<i>rand</i>	Value between 0 and 1
LB_j	jth minimum limit
UB_j	jth maximum limit
$X_1(t+1)$	Solution of the following generation of t
$X_{best}(t)$	Superior solution of i th generation
X_M	Mean value of location
X_R	Random solution between 1 and N
D	Dimension search size
$Levy(D)$	Levy flight division function
S	Fixed value of 0.01
r_1	Value from 1 to 20 during the search cycles
U	Value of 0.00565
$QF(t)$	Quality function

References

- Gao, F.; Hu, R.; Yin, L. Variable boundary reinforcement learning for maximum power point tracking of photovoltaic grid-connected systems. *Energy* **2023**, *264*, 126278. [[CrossRef](#)]
- Farayola, A.M.; Sun, Y.; Ali, A. Global maximum power point tracking and cell parameter extraction in Photovoltaic systems using improved firefly algorithm. *Energy Rep.* **2022**, *8*, 162–186. [[CrossRef](#)]
- Guo, A.; Xu, Y.; Rezvani, A. Performance improvement of maximum power point tracking for photovoltaic system using grasshopper optimization algorithm based ANFIS under different conditions. *Optik* **2022**, *270*, 169965. [[CrossRef](#)]
- Perin Gasparin, F.; Detzel Kipper, F.; Schuck de Oliveira, F.; Krenzinger, A. Assessment on the variation of temperature coefficients of photovoltaic modules with solar irradiance. *Sol. Energy* **2022**, *244*, 126–133. [[CrossRef](#)]
- Osmani, K.; Haddad, A.; Lemenand, T.; Castanier, B.; Ramadan, M. An investigation on maximum power extraction algorithms from PV systems with corresponding DC-DC converters. *Energy* **2021**, *224*, 120092. [[CrossRef](#)]
- Islam, H.; Mekhilef, S.; Shah, N.M.; Soon, T.K.; Wahyudie, A.; Ahmed, M. Improved proportional-integral coordinated MPPT controller with fast tracking speed for grid-tied PV systems under partially shaded conditions. *Sustainability* **2021**, *13*, 830. [[CrossRef](#)]
- Kumar, V.; Bindal, R.K. MPPT technique used with perturb and observe to enhance the efficiency of a photovoltaic system. *Mater. Today Proc.* **2022**, *69*, A6–A11. [[CrossRef](#)]
- Kumar, P.; Shrivastava, A. Maximum power tracking from solar PV system by using fuzzy-logic and incremental conductance techniques. *Mater. Today Proc.* **2022**, *79*, 267–277. [[CrossRef](#)]
- Leelavathi, M.; Suresh Kumar, V. Deep neural network algorithm for MPPT control of double diode equation-based PV module. *Mater. Today Proc.* **2022**, *62*, 4764–4771. [[CrossRef](#)]
- Doubabi, H.; Salhi, I.; Chennani, M.; Essounbouli, N. High Performance MPPT based on TS Fuzzy–integral backstepping control for PV system under rapid varying irradiance—Experimental validation. *ISA Trans.* **2021**, *118*, 247–259. [[CrossRef](#)]
- Srinivasan, V.; Boopathi, C.S.; Sridhar, R. A new meerkat optimization algorithm based maximum power point tracking for partially shaded photovoltaic system. *Ain Shams Eng. J.* **2021**, *12*, 3791–3802. [[CrossRef](#)]
- Pandey, A.K.; Singh, V.; Jain, S. Study and comparative analysis of perturb and observe (P&O) and fuzzy logic based PV-MPPT algorithms. In *Applications of AI and IOT in Renewable Energy*; Academic Press: Cambridge, MA, USA, 2022. [[CrossRef](#)]
- Ram, J.P.; Pillai, D.S.; Ghias AM, Y.M.; Rajasekar, N. Performance enhancement of solar PV systems applying P&O assisted Flower Pollination Algorithm (FPA). *Sol. Energy* **2020**, *199*, 214–229. [[CrossRef](#)]
- Dorji, S.; Wangchuk, D.; Choden, T.; Tshewang, T. Maximum power point tracking of solar photovoltaic cell using perturb observe and fuzzy logic controller algorithm for boost converter and quadratic boost converter. *Mater. Today Proc.* **2020**, *27*, 1224–1229. [[CrossRef](#)]
- Mathi, D.K.; Chinthamalla, R. A hybrid global maximum power point tracking method based on butterfly particle swarm optimization and perturb and observe algorithms for a photovoltaic system under partially shaded conditions. *Int. Trans. Electr. Energy Syst.* **2020**, *30*, e12543. [[CrossRef](#)]
- Bhan, V.; Shaikh, S.A.; Khand, Z.H.; Ahmed, T.; Khan, L.A.; Chachar, F.A.; Shaikh, A.M. Performance Evaluation of Perturb and Observe Algorithm for MPPT with Buck–Boost Charge Controller in Photovoltaic Systems. *J. Control. Autom. Electr. Syst.* **2021**, *32*, 1652–1662. [[CrossRef](#)]
- Alagammal, S.; Rathina Prabha, N. Combination of Modified P&O with Power Management Circuit to Exploit Reliable Power from Autonomous PV-Battery Systems. *Iran. J. Sci. Technol.-Trans. Electr. Eng.* **2021**, *45*, 97–114. [[CrossRef](#)]
- Mohammadinodoushan, M.; Abbassi, R.; Jerbi, H.; Ahmed, F.W.; Ahmed, H.A.K.; Rezvani, A. A new MPPT design using variable step size perturb and observe method for PV system under partially shaded conditions by modified shuffled frog leaping algorithm-SMC controller. *Sustain. Energy Technol. Assess.* **2021**, *45*, 101056. [[CrossRef](#)]
- Ahmed, N.A.; Abdul Rahman, S.; Alajmi, B.N. Optimal controller tuning for P&O maximum power point tracking of PV systems using genetic and cuckoo search algorithms. *Int. Trans. Electr. Energy Syst.* **2021**, *31*, e12624. [[CrossRef](#)]

20. Jiang, M.; Ghahremani, M.; Dadfar, S.; Chi, H.; Abdallah, Y.N.; Furukawa, N. A novel combinatorial hybrid SFL-PS algorithm based neural network with perturb and observe for the MPPT controller of a hybrid PV-storage system. *Control Eng. Pract.* **2021**, *114*, 104880. [[CrossRef](#)]
21. Abdel-Salam, M.; El-Mohandes, M.T.; El-Ghazaly, M. An Efficient Tracking of MPP in PV Systems Using a Newly-Formulated P&O-MPPT Method Under Varying Irradiation Levels. *J. Electr. Eng. Technol.* **2020**, *15*, 501–513. [[CrossRef](#)]
22. Tali, S.A.; Ahmad, F.; Wani, I.H. Hardware implementation of improved perturb and observe maximum power point tracking technique for photovoltaic systems with zero oscillations. *Analog Integr. Circuits Signal Process.* **2022**, *112*, 13–18. [[CrossRef](#)]
23. Siva Kumar, C.H.; Mallesham, G. A new hybrid boost converter with P & O MPPT for high gain enhancement of solar PV system. *Mater. Today Proc.* **2022**, *57*, 2262–2269. [[CrossRef](#)]
24. Abdel-Salam, M.; El-Mohandes, M.T.; Goda, M. An improved perturb-and-observe based MPPT method for PV systems under varying irradiation levels. *Sol. Energy* **2018**, *171*, 547–561. [[CrossRef](#)]
25. Ali, Z.M.; Vu Quynh, N.; Dadfar, S.; Nakamura, H. Variable step size perturb and observe MPPT controller by applying θ -modified krill herd algorithm-sliding mode controller under partially shaded conditions. *J. Clean. Prod.* **2020**, *271*, 122243. [[CrossRef](#)]
26. Ali AI, M.; Mohamed HR, A. Improved P&O MPPT algorithm with efficient open-circuit voltage estimation for two-stage grid-integrated PV system under realistic solar radiation. *Int. J. Electr. Power Energy Syst.* **2022**, *137*, 107805. [[CrossRef](#)]
27. Da Rocha, M.V.; Sampaio, L.P.; da Silva SA, O. Comparative analysis of MPPT algorithms based on Bat algorithm for PV systems under partial shading condition. *Sustain. Energy Technol. Assess.* **2020**, *40*, 100761. [[CrossRef](#)]
28. Shang, L.; Guo, H.; Zhu, W. An improved MPPT control strategy based on incremental conductance algorithm. *Prot. Control Mod. Power Syst.* **2020**, *5*, 14. [[CrossRef](#)]
29. Li, S.; Li, F.; Zheng, J.; Chen, W.; Zhang, D. An improved MPPT control strategy based on incremental conductance method. *Soft Comput.* **2020**, *24*, 6039–6046. [[CrossRef](#)]
30. Ahmed, E.M.; Norouzi, H.; Alkhafaf, S.; Ali, Z.M.; Dadfar, S.; Furukawa, N. Enhancement of MPPT controller in PV-BES system using incremental conductance along with hybrid crow-pattern search approach based ANFIS under different environmental conditions. *Sustain. Energy Technol. Assess.* **2022**, *50*, 101812. [[CrossRef](#)]
31. Mishra, J.; Das, S.; Kumar, D.; Pattnaik, M. A novel auto-tuned adaptive frequency and adaptive step-size incremental conductance MPPT algorithm for photovoltaic system. *Int. Trans. Electr. Energy Syst.* **2021**, *31*, e12813. [[CrossRef](#)]
32. Singh, P.; Shukla, N.; Gaur, P. Modified variable step incremental-conductance MPPT technique for photovoltaic system. *Int. J. Inf. Technol.* **2021**, *13*, 2483–2490. [[CrossRef](#)]
33. Sheikh Ahmadi, S.H.; Karami, M.; Gholami, M.; Mirzaei, R. Improving MPPT Performance in PV Systems Based on Integrating the Incremental Conductance and Particle Swarm Optimization Methods. *Iran. J. Sci. Technol.-Trans. Electr. Eng.* **2022**, *46*, 27–39. [[CrossRef](#)]
34. Karafil, A. Thinned-out controlled IC MPPT algorithm for class E resonant inverter with PV system. *Ain Shams Eng. J.* **2023**, *14*, 101992. [[CrossRef](#)]
35. Jagadeshwar, M.; Dushmanta, K.D. A Novel Adaptive Model Predictive Control Scheme with Incremental Conductance for Extracting Maximum Power from a Solar Panel. *Iran. J. Sci. Technol. Trans. Electr. Eng.* **2023**, *46*, 653–664. [[CrossRef](#)]
36. Singh, D.K.; Akella, A.K.; Manna, S. A novel robust maximum power extraction framework for sustainable PV system using incremental conductance based MRAC technique. *Environ. Prog. Sustain. Energy* **2023**, *42*, e14137. [[CrossRef](#)]
37. Chauhan, U.; Chhabra, H.; Rani, A.; Kumar, B.; Singh, V. Efficient MPPT Controller for Solar PV System Using GWO-CS Optimized Fuzzy Logic Control and Conventional Incremental Conductance Technique. *Iran. J. Sci. Technol.-Trans. Electr. Eng.* **2022**, *47*, 463–472. [[CrossRef](#)]
38. Bouarroudj, N.; Benlahbib, B.; Sedraoui, M.; Feliu-Batlle, V.; Bechouat, M.; Boukhetala, D.; Boudjema, F. A new tuning rule for stabilized integrator controller to enhance the indirect control of incremental conductance MPPT algorithm: Simulation and practical implementation. *Optik* **2022**, *268*, 169728. [[CrossRef](#)]
39. Hiyama, T.; Kitabayashi, K. Neural network based estimation of maximum power generation from PV module using environmental information. *IEEE Trans. Energy Convers.* **1997**, *12*, 241–247. [[CrossRef](#)]
40. Bahgat AB, G.; Helwa, N.H.; Ahmad, G.E.; el Shenawy, E.T. Maximum power point traking controller for PV systems using neural networks. *Renew. Energy* **2005**, *30*, 1257–1268. [[CrossRef](#)]
41. Asiful Islam, M.; Ashfanoor Kabir, M. Neural network based maximum power point tracking of photovoltaic arrays. In *IEEE Region 10 Annual International Conference, Proceedings/TENCON*; IEEE: Piscataway, NJ, USA, 2011. [[CrossRef](#)]
42. Kurniawan, A.; Shintaku, E. A Neural Network-Based Rapid Maximum Power Point Tracking Method for Photovoltaic Systems in Partial Shading Conditions. *Appl. Sol. Energy* **2020**, *56*, 157–167. [[CrossRef](#)]
43. Ibelouad, A.; el Kari, A.; Ayad, H.; Mjahed, M. Improved cooperative artificial neural network-particle swarm optimization approach for solar photovoltaic systems using maximum power point tracking. *Int. Trans. Electr. Energy Syst.* **2020**, *30*, e12439. [[CrossRef](#)]
44. Fathi, M.; Parian, J.A. Intelligent MPPT for photovoltaic panels using a novel fuzzy logic and artificial neural networks based on evolutionary algorithms. *Energy Rep.* **2021**, *7*, 1338–1348. [[CrossRef](#)]
45. Hamdi, H.; ben Regaya, C.; Zaafouri, A. Real-time study of a photovoltaic system with boost converter using the PSO-RBF neural network algorithms in a MyRio controller. *Sol. Energy* **2019**, *183*, 1–16. [[CrossRef](#)]

46. Rao, C.V.; Raj RD, A.; Anil Naik, K. A novel hybrid image processing-based reconfiguration with RBF neural network MPPT approach for improving global maximum power and effective tracking of PV system. *Int. J. Circuit Theory Appl.* **2023**, *51*, 4397–4426. [[CrossRef](#)]
47. Haq, I.U.; Khan, Q.; Ullah, S.; Khan, S.A.; Akmeliaiwati, R.; Khan, M.A.; Iqbal, J. Neural network-based adaptive global sliding mode MPPT controller design for stand-alone photovoltaic systems. *PLoS ONE* **2022**, *17*, e0260480. [[CrossRef](#)]
48. Won, C.Y.; Kim, D.H.; Kim, S.C.; Kim, W.S.; Kim, H.S. New maximum power point tracker of photovoltaic arrays using fuzzy controller. *PESC Rec.-IEEE Annu. Power Electron. Spec. Conf.* **1994**, *1*, 396–403. [[CrossRef](#)]
49. Asif, R.M.; Ur Rehman, A.; Ur Rehman, S.; Arshad, J.; Hamid, J.; Tariq Sadiq, M.; Tahir, S. Design and analysis of robust fuzzy logic maximum power point tracking based isolated photovoltaic energy system. *Eng. Rep.* **2020**, *2*, e12234. [[CrossRef](#)]
50. Veeramanikandan, P.; Selvaperumal, S. Investigation of different MPPT techniques based on fuzzy logic controller for multilevel DC link inverter to solve the partial shading. *Soft Comput.* **2021**, *25*, 3143–3154. [[CrossRef](#)]
51. Senthilnathan, A.; Murugasami, R.; Balakrishnan, R.; Sundar, R.; Palanivel, P. Fuzzy logic controlled 3 port DC to DC Cuk converter with IoT based PV panel monitoring system. *Int. J. Syst. Assur. Eng. Manag.* **2022**, *1*–9. [[CrossRef](#)]
52. Hai, T.; Zhou, J.; Muranaka, K. An efficient fuzzy-logic based MPPT controller for grid-connected PV systems by farmland fertility optimization algorithm. *Optik* **2022**, *267*, 169636. [[CrossRef](#)]
53. Daraban, S.; Petreus, D.; Morel, C. A novel MPPT (maximum power point tracking) algorithm based on a modified genetic algorithm specialized on tracking the global maximum power point in photovoltaic systems affected by partial shading. *Energy* **2014**, *74*, 374–388. [[CrossRef](#)]
54. Hashim, N.; Salam, Z.; Ayob, S.M. Maximum power point tracking for stand-alone photovoltaic system using evolutionary programming. In Proceedings of the 2014 IEEE 8th International Power Engineering and Optimization Conference, PEOCO, Langkawi, Malaysia, 24–25 March 2014. [[CrossRef](#)]
55. Ramasamy, S.; Jeevananthan, S.; Dash, S.S.; Selvan, T. An intelligent differential evolution based maximum power point tracking (MPPT) technique for partially shaded photo voltaic (PV) array. *Int. J. Adv. Soft Comput. Its Appl.* **2014**, *6*, 1–16.
56. Manmadharao, T.; Balamurali, P.; Ravikumar, C. Maximum power point tracking of a PV system by Bacteria foraging oriented Particle Swarm optimization. *Int. J. Eng. Res. Gen. Sci.* **2015**, *3*, 515–524.
57. Ahmed, J.; Salam, Z. A Maximum Power Point Tracking (MPPT) for PV system using Cuckoo Search with partial shading capability. *Appl. Energy* **2014**, *119*, 118–130. [[CrossRef](#)]
58. Benyoucef A soufyane Chouder, A.; Kara, K.; Silvestre, S.; Sahed, O.A. Artificial bee colony based algorithm for maximum power point tracking (MPPT) for PV systems operating under partial shaded conditions. *Appl. Soft Comput. J.* **2015**, *32*, 38–48. [[CrossRef](#)]
59. Jiang, L.L.; Maskell, D.L.; Patra, J.C. A novel ant colony optimization-based maximum power point tracking for photovoltaic systems under partially shaded conditions. *Energy Build.* **2013**, *58*, 227–236. [[CrossRef](#)]
60. Safarudin, Y.M.; Priyadi, A.; Purnomo, M.H.; Pujiantara, M. Maximum power point tracking algorithm for photovoltaic system under partial shaded condition by means updating β firefly technique. In Proceedings of the 2014 6th International Conference on Information Technology and Electrical Engineering: Leveraging Research and Technology Through University-Industry Collaboration, ICITEE, Yogyakarta, Indonesia, 7–8 October 2014. [[CrossRef](#)]
61. Mach, J.B.; Ronoh, K.K.; Langat, K. Improved spectrum allocation scheme for TV white space networks using a hybrid of firefly, genetic, and ant colony optimization algorithms. *Heliyon* **2023**, *9*, e13752. [[CrossRef](#)]
62. Lyden, S.; Haque, M.E.; Xiao, D. Application of a Simulated Annealing technique for global maximum power point tracking of PV modules experiencing partial shading. In *IECON Proceedings (Industrial Electronics Conference)*; IEEE: Piscataway, NJ, USA, 2014. [[CrossRef](#)]
63. Mohd Yusof, N.; Muda, A.K.; Pratama, S.F.; Carbo-Dorca, R.; Abraham, A. Improving Amphetamine-type Stimulants drug classification using chaotic-based time-varying binary whale optimization algorithm. *Chemom. Intell. Lab. Syst.* **2022**, *229*, 104635. [[CrossRef](#)]
64. Manoochehr Makvandi Neissi, N.; Tarighi, P.; Makvandi, K.; Rashidi, N. Evaluation of the Genes Expression Related to the Immune System in Response to Helicobacter pylori Catalase Epitopes. *Mol. Genet. Microbiol. Virol.* **2020**, *35*, 47–51. [[CrossRef](#)]
65. Barr, R.S.; Glover, F.; Huskinson, T.; Kochenberger, G. An extreme-point tabu-search algorithm for fixed-charge network problems. *Networks* **2021**, *77*, 322–340. [[CrossRef](#)]
66. Saleem, O.; Awan, F.G.; Mahmood-ul-Hasan, K.; Ahmad, M. Self-adaptive fractional-order LQ-PID voltage controller for robust disturbance compensation in DC-DC buck converters. *Int. J. Numer. Model.* **2020**, *33*, e2718. [[CrossRef](#)]
67. Youcef, D.; Khatir, K.; Yassine, B. Design of neural network fractional-order backstepping controller for MPPT of PV systems using fractional-order boost converter. *Int Trans Electr Energ Syst.* **2021**, *31*, e13188. [[CrossRef](#)]
68. Chen, X.; Chen, Y.; Zhang, B.; Qiu, D. A modeling and analysis method for fractional-order DC–DC converters. *IEEE Trans. Power Electron.* **2016**, *32*, 7034–7044. [[CrossRef](#)]
69. Ni, J.; Xiang, J. A Concise Control Method Based on Spatial-Domain dp/dv Calculation for MPPT/Power Reserved of PV Systems. *IEEE Trans. Energy Convers.* **2023**, *38*, 3–14. [[CrossRef](#)]
70. Park, H.E.; Song, J.H. A dP/dV feedback-controlled MPPT method for photovoltaic power system using II-SEPIC. *J. Power Electron.* **2009**, *9*, 604–611.
71. Douris, A.I.; Kofinas, P.; Alafodimos, C.; Tseles, D. Adaptive fuzzy gain scheduling PID controller for maximum power point tracking of photovoltaic system. *Renew. Energy* **2013**, *60*, 202–214. [[CrossRef](#)]

72. Dounis, A.I.; Stavrinidis, S.; Kofinas, P.; Tseles, D. Fuzzy-PID controller for MPPT of PV system optimized by Big Bang-Big Crunch algorithm. In Proceedings of the IEEE International Conference on Fuzzy Systems, Istanbul, Turkey, 2–5 November 2015. [[CrossRef](#)]
73. Ashok Kumar, B.; Srinivasa Venkatesh, M.; Mohan Muralikrishna, G. Optimization of photovoltaic power using PID MPPT controller based on incremental conductance algorithm. *Lect. Notes Electr. Eng.* **2015**, *326*, 803–809. [[CrossRef](#)]
74. Kler, D.; Rana KP, S.; Kumar, V. A nonlinear PID controller based novel maximum power point tracker for PV systems. *J. Frankl. Inst.* **2018**, *355*, 7827–7864. [[CrossRef](#)]
75. Long, B.; Lu, P.; Zhan, D.; Lu, X.; Rodríguez, J.; Guerrero, J.M.; Chong, K. Adaptive fuzzy fractional-order sliding-mode control of LCL-interfaced grid-connected converter with reduced-order. *ISA Trans.* **2023**, *132*, 557–572. [[CrossRef](#)]
76. Ahmed, W.A.E.M.; Mageed, H.M.A.; Mohamed, S.A.E.; Saleh, A.A. Fractional order Darwinian particle swarm optimization for parameters identification of solar PV cells and modules. *Alex. Eng. J.* **2022**, *61*, 1249–1263. [[CrossRef](#)]
77. Yang, B.; Yu, T.; Shu, H.; Zhu, D.; An, N.; Sang, Y.; Jiang, L. Perturbation observer based fractional-order sliding-mode controller for MPPT of grid-connected PV inverters: Design and real-time implementation. *Control. Eng. Pract.* **2018**, *79*, 105–125. [[CrossRef](#)]
78. Monje C a Chen, Y.Q.; Vinagre, B.M.; Xue, D.; Feliu, V. *Fractional-order Systems and Controls. Fundamentals and Applications*; Springer-Verlag: London, UK, 2010. [[CrossRef](#)]
79. Raheem, F.S.; Basil, N. Automation intelligence photovoltaic system for power and voltage issues based on Black Hole Optimization algorithm with FOPIID. *Meas. Sens.* **2023**, *25*, 100640. [[CrossRef](#)]
80. Abualigah, L.; Yousri, D.; Abd Elaziz, M.; Ewees, A.A.; Al-qaness MA, A.; Gandomi, A.H. Aquila Optimizer: A novel meta-heuristic optimization algorithm. *Comput. Ind. Eng.* **2021**, *157*, 107250. [[CrossRef](#)]

Disclaimer/Publisher's Note: The statements, opinions and data contained in all publications are solely those of the individual author(s) and contributor(s) and not of MDPI and/or the editor(s). MDPI and/or the editor(s) disclaim responsibility for any injury to people or property resulting from any ideas, methods, instructions or products referred to in the content.